

REPORT DOCUMENTATION PAGE

AFRL-SR-AR-TR-06-0463

The public reporting burden for this collection of information is estimated to average 1 hour per response, including gathering and maintaining the data needed, and completing and reviewing the collection of information. Send comment of information, including suggestions for reducing the burden, to Department of Defense, Washington Headquarters (0704-0188), 1215 Jefferson Davis Highway, Suite 1204, Arlington, VA 22202-4302. Respondents should be aware that providing information is required by law and that failure to provide information may result in the imposition of a civil or criminal penalty. Please do not return your form to the above address.

1. REPORT DATE (DD-MM-YYYY)		2. REPORT TYPE FINAL REPORT		3. DATES COVERED (From - To) 01 May 2003 - 30 Apr 2006	
4. TITLE AND SUBTITLE DONOR, ACCEPTORS AND TRAPS IN ALGAN AND ALGAN/GAN EPITAXIAL LAYERS				5a. CONTRACT NUMBER	
				5b. GRANT NUMBER F49620-03-1-0197	
				5c. PROGRAM ELEMENT NUMBER 61102F	
6. AUTHOR(S) DR LOOK				5d. PROJECT NUMBER 2305/BX	
				5e. TASK NUMBER BX	
				5f. WORK UNIT NUMBER	
7. PERFORMING ORGANIZATION NAME(S) AND ADDRESS(ES) WRIGHT STATE UNIVERSITY 3640 COL GLENN HWY DAYTON OH 45435-0001				8. PERFORMING ORGANIZATION REPORT NUMBER	
9. SPONSORING/MONITORING AGENCY NAME(S) AND ADDRESS(ES) AIR FORCE OF SCIENTIFIC RESEARCH AFOSR/NE 875 NORTH RANDOLPH STREET SUITE 325 ROOM 3112 ARLINGTON VA 22203-1768 <i>Dr Gerald Witt</i>				10. SPONSOR/MONITOR'S ACRONYM(S)	
				11. SPONSOR/MONITOR'S REPORT NUMBER(S)	
12. DISTRIBUTION/AVAILABILITY STATEMENT DISTRIBUTION STATEMENT A: UNLIMITED					
13. SUPPLEMENTARY NOTES					
14. ABSTRACT The Wood-Witt program was organized in 1999, and has involved more than fifty participants, from more than ten different countries. The present grant, F49620-03-1-0197, has covered the period 1May03 - 30Apr06. The overall goal has been to understand defects and impurities in GaN, and determine how to reduce them, if possible. More than 600 GaN samples have been investigated in our laboratory or sent out since the inception of the program, and much has been learned about this important material. The participants from Wright State University (WSU) during the last three years have included Bruce (Chip) Claflin, Timothy Cooper, Zhaoqiang Fang, Gary Farlow, John Hoelscher, Brahmanand (Val) Jogai, David Look, Donald Reynolds, and Wallace Rice, Jr. There have also been participatns from the Materials and Manufacturing Directorate, and Sensors Directorate of the Air Force Research Laboratory (AFRL), and many others from around the world. We especially want to thank our AFOSR program managers, Dr. Gerald L. Witt, who initiated the program, Dr. Kitt C. Reinhardt, who took over near the end. Their insight and support has been crucial in making this program successful. One measure of success is the number and quantity of journal publications resulting from the research. Any questions or comments to Dr. David Look, David.look@wright.edu.					
15. SUBJECT TERMS ALGAN/GAN					
16. SECURITY CLASSIFICATION OF:			17. LIMITATION OF ABSTRACT	18. NUMBER OF PAGES	19a. NAME OF RESPONSIBLE PERSON
a. REPORT U	b. ABSTRACT U	c. THIS PAGE U			19b. TELEPHONE NUMBER (include area code)

03NE 089
06 00222

Wright State University:
Semiconductor
Research Center

134 Oelman Hall
3640 Col. Glenn Hwy.
Dayton OH 45435

Final Technical Report

to

Air Force Office of Scientific Research

Attn: Dr. Kitt C. Reinhardt
Physics & Electronics Directorate, AFOSR/NE
875 North Randolph Street, Suite 325, Room 3112
Arlington, VA 22203
kitt.reinhardt@afosr.af.mil

**Title: Donors, Acceptors, and Traps in AlGa_N and
AlGa_N/Ga_N Epitaxial Layers**

Grant F49620-03-1-0197

Principle Investigator

Dr. David C. Look, david.look@wright.edu

Date of report: 31July06
Period of report: 1May03 – 30Apr06
Period of grant: 1May03 – 30Apr06

20061130018

Foreword

The Wood-Witt program was organized in 1999, and has involved more than fifty participants, from more than ten different countries. The present grant, F49620-03-1-0197, has covered the period 1May03 – 30Apr06. The overall goal has been to understand defects and impurities in GaN, and determine how to reduce them, if possible. More than 600 GaN samples have been investigated in our laboratory or sent out since the inception of the program, and much has been learned about this important material. The participants from Wright State University (WSU) during the last three years have included Bruce (Chip) Claflin, Timothy Cooper, Zhaoqiang Fang, Gary Farlow, John Hoelscher, Brahmanand (Val) Jogai, David Look, Donald Reynolds, and Wallace Rice, Jr. There have also been participants from the Materials and Manufacturing Directorate, and Sensors Directorate of the Air Force Research Laboratory (AFRL), and many others from around the world. We especially want to thank our AFOSR program managers, Dr. Gerald L. Witt, who initiated the program, Dr. Kitt C. Reinhardt, who took over near the end. Their insight and support has been crucial in making this program successful. One measure of success is the number and quality of journal publications resulting from the research. In the last three years, our group at WSU has generated twenty-five papers, co-authored by scientists in ten different countries. Also, many additional papers from other groups have been published on the same set of samples. A list of the WSU publications is included at the end of this report. We have also chosen three topics to illustrate in more detail in the body of the report, below. Each of the three sections is self contained, and thus can be read without reference to either of the other two. Any questions or comments on the research can be directed to Dr. David Look, david.look@wright.edu.

Table of Contents

1.0	The nitrogen vacancy in GaN	Page 4
2.0	Giant traps associated with extended defects in GaN and SiC	Page 11
3.0	Characterization of bulk-like GaN grown by hydride vapor phase epitaxy	Page 23
4.0	List of Publications	Page 34

1.0 The nitrogen vacancy in GaN

1.1 Introduction

The last decade has seen greatly increased research and development on GaN-related materials and devices.¹ The driving force has been the potential for blue/UV light-emitting diodes (LEDs) and laser diodes (LDs), and also high-frequency transistors operating at high powers and temperatures. Much of the GaN research has concentrated on identifying impurities and defects that may act as donors, acceptors, traps, or recombination centers.² In particular, the main donors that have been investigated so far are oxygen occupying a nitrogen site (O_N), silicon on a Ga site (Si_{Ga}), and the N vacancy.^{3,4} Several years ago, we performed 0.7 – 1.0 MeV electron irradiation on the best (highest-mobility) GaN samples available at that time, and found that a donor (at 64 ± 10 meV below the conduction-band edge) and an acceptor (much lower in the bandgap) were produced at approximately the same rate. We then used several arguments to assign the donor to the N vacancy, and the acceptor to the N interstitial.⁴ Recently, GaN samples with much lower background donor and acceptor concentrations have become available, allowing better accuracy in the Hall fitting, and sharper and more intense photoluminescence (PL) spectra.⁵⁻⁷ Furthermore, we have gained access to a lower-energy electron accelerator, allowing a separation of N-sublattice from Ga-sublattice damage. Thus, we have revisited the GaN defect problem by irradiating this new, higher-quality GaN with 0.42-MeV electrons, which recent displacement-energy calculations have shown to be above the N-sublattice damage threshold, but below that of the Ga sublattice.⁸ Therefore, in this case, we can be sure that only N vacancies (V_N) and interstitials (N_I) are initially being produced by the irradiation. However, the N_I are likely mobile at room temperature, either recombining with vacancies, or forming complexes with existing impurities or defects. One of these irradiated samples was given to a group performing PL measurements, and new, weak lines were seen in the donor-bound exciton (DBE) region and the two-electron satellite (TES) region. By assuming that the DBE and TES lines represented, respectively, $n=1$ and $n=2$ final states of the same donor, it was concluded that a 25-meV donor was being created by the irradiation. Furthermore, this donor was assigned to the N vacancy. However, we show below that this assignment is completely incompatible with our Hall results, since donors in the 25-meV region actually *decrease* in concentration, and is also incompatible with our PL results, since no new DBE lines are observed in our irradiated sample.

1.2 Experimental considerations

The GaN sample discussed here was grown in the (0001) orientation (Ga face up) on Al₂O₃ by the hydride vapor-phase epitaxial (HVPE) technique at the Samsung Advanced Institute of Technology.⁵ Separation of the GaN and Al₂O₃ was effected by laser irradiation on the N face, through the Al₂O₃ substrate. Lapping and polishing of both the Ga and N faces produced a flat sample of thickness 219 μm. This process also removed the highly-conductive N-face/Al₂O₃ interface layer, which made analysis difficult in our first study.⁴ Samples of this type have been extensively characterized by optical, electrical, and structural techniques,⁵⁻⁷ and have demonstrated record mobilities.⁶

The van der Pauw Hall-effect measurements were performed with a LakeShore Model 7507 apparatus, including a closed-cycle He cooling system operating from 15 – 320 K. From measurements of Hall coefficient R and conductivity σ , the Hall mobility $\mu_H = R\sigma$ and the Hall concentration $n_H = 1/eR$ could be calculated at each temperature. The true carrier concentration n is related to n_H by $n = rn_H$, where r is the so-called Hall r -factor.⁹ For the unirradiated sample, $r = 1.1 - 1.3$, from 50 – 320 K, and for the irradiated sample, $r = 1.1 - 1.5$.

Photoluminescence measurements were performed at 4.2 K. Excitation, dispersion, and detection were accomplished, respectively, with a 45-mW HeCd laser, a 1.25-m spectrometer, and a photomultiplier detector. Resolution was better than 0.01 meV in the spectral range important for this study. Electron irradiations were carried out at room temperature with the beam directed in the [000-1] direction, i.e., opposite to the growth direction. The energy was about 0.42 MeV, the current about 2 μA/cm², and the total fluence about 3.6 x 10¹⁷ cm⁻². Very recently, threshold displacement energies (E_d 's) have been calculated for GaN using realistic potentials.⁸ Depending on irradiation direction, the *minimum* E_d for N displacement is 25 eV, and that for Ga displacement, 22 eV. However, along the [000-1] direction, and averaging over a 15 ° acceptance angle to account for thermal motions and possible beam misalignment, the calculated E_d 's are 66 and 38 eV, respectively, for N and Ga displacements.¹⁰ From these theoretical results, and accounting for the higher mass of Ga, it is found that the minimum electron energy needed for N displacement is 0.32 MeV, and for Ga displacement, 0.53 MeV. Furthermore, using the McKinley-Feshbach relativistic displacement-cross-section formula,⁴ the N production rate should be about 0.03 cm⁻¹ at our electron energy of 0.42 MeV, and will exceed the Ga production rate up to electron energies of 0.87 MeV. These considerations support our conclusion that the present irradiations are primarily producing N-sublattice displacements. Ga-sublattice displacements have been identified in irradiations at much higher energies, e.g., 2.0 – 2.5 MeV.^{11,12} However, the Ga interstitial Ga_i is mobile at room temperature, and tends

to form complexes.¹³ Furthermore, only tightly-bound wave functions have been associated with Ga_i.^{11,13} Thus, the isolated Ga_i is not a good candidate for the shallow donor produced by room-temperature irradiation, and the Ga vacancy is, of course, not a donor at all, but a well-known acceptor.¹² From these results, only the N vacancy is a reasonable candidate for the shallow donor produced by 0.42-MeV electron irradiation.

1.3 Results

The temperature dependence of carrier concentration n and mobility μ are shown in Fig. 1. The peak mobility is mainly sensitive to the acceptor concentration N_A , showing that N_A increases with irradiation.^{4,9} Note that N_A is the *total* acceptor concentration, including the original acceptors as well as those produced by the irradiation. (From the Hall-effect measurements, we cannot determine the energy levels of the acceptors, except that they must be at least several kT below the donor levels.) In Fig. 1, it is clearly seen that another, deeper donor N_{D2} has been produced by the irradiation, although the original, shallower donor N_{D1} is also still present. The fitted values of N_{D1} , E_{D1} , N_{D2} , E_{D2} , and N_A are given in Table 1. Here, N_A is determined from the mobility data, and all the other parameters from the carrier-concentration data.⁹ Note that a donor at 70 ± 2 meV increases in concentration by $7.0 \times 10^{15} \text{ cm}^{-3}$, giving a production rate of about 0.02 cm^{-1} , close to the predicted value of 0.03 cm^{-1} . In contrast, the donors at 25 ± 1 meV actually *decrease* in concentration, by $1.8 \times 10^{15} \text{ cm}^{-3}$. This observation can be understood by realizing that the N interstitials are likely mobile at room temperature, and will tend to form complexes with impurities or other defects. Since the main donor impurity in the present material is probably O_N ,⁷ a single donor, and since N_I is thought to be a single acceptor in n-type GaN,¹⁴ there would be a coulomb attraction between O_N and N_I , and the resulting complex O_N-N_I would probably be neutral. This process could explain why the 25-meV donors decrease in concentration. In this scenario, the remaining N_I (of concentration $5.2 \times 10^{15} \text{ cm}^{-3}$) would account for the increase in acceptor concentration ($3.0 \times 10^{15} \text{ cm}^{-3}$), and also a possible increase in some other neutral centers, not associated with the original shallow donors.

It is interesting to compare the present donor energy of 70 ± 2 meV with the value 64 ± 10 meV deduced in the earlier irradiation study.⁴ In the earlier case, the background donor concentration was $1.2 \times 10^{17} \text{ cm}^{-2}$, whereas the background donor concentration in the present sample is $1.25 \times 10^{16} \text{ cm}^{-3}$. Using the screening formula, $E_D = E_{D0} - \alpha N_D^{1/3}$, with $\alpha = 2.1 \times 10^{-5} \text{ meV-cm}$,¹⁵ we get an unscreened energy $E_{D0} = 75$

meV in the present study, and 74 meV in the former study. Thus, there is no doubt that the defect donors produced at 0.42 MeV, and those produced at 0.7 – 1.0 MeV, are the same.

1.4 Discussion

A recent paper by Yang et al. (henceforth called YFW),¹⁶ based on a nearly identical irradiated sample, concludes that an optically-observed 25-meV center is the N vacancy. This assignment is immediately incompatible with our results in that the donors at 25 ± 1 meV actually *decrease* in concentration. Furthermore, we can compare the YFW PL data with our own PL data. In Fig. 2, we present donor-bound exciton spectra from three different samples: (1) unirradiated S422 (dashed line); (2) irradiated S422 (solid line); and (3) unirradiated S417 (chained line). Here, sample S417 is shown for comparison, since YFW had an adjacent piece of S417. Note the three well-defined DBE lines in S417, at 3.47136, 3.47241, and 3.47319 eV, respectively. The identity of the first of these is unknown, whereas the other two are usually assigned to O_N and Si_{Ga} , respectively.^{3,7,17} The unirradiated and irradiated S422 samples exhibit the same three lines, but they are not as sharply defined. In their unirradiated sample S417, YFW find the dominant line (O_N) at 3.4717 eV, and the Si_{Ga} line at 3.4725 eV, each about 0.7 meV below our corresponding values, due to a different spectrometer calibration. But after irradiation, they find a new line, at 3.4732 eV. The O_N , Si_{Ga} , and new line, each raised by 0.7 meV to match our O_N and Si_{Ga} lines, are schematically represented by solid vertical lines in Fig. 2. Clearly, we do not see their new DBE line in our irradiated sample. However, they also observe another weak line produced by the irradiation, at 3.4547 eV (not shown), and this they believe is the so-called two-electron satellite (TES) line of the new DBE line at 3.4732. (Note that TES lines result from bound-exciton transitions in which the donor is left in an $n=2$ state.) Then, by applying the hydrogenic model to the DBE ($n=1$) and TES ($n=2$) lines, the defect donor energy becomes $4/3(3.4732 - 3.4547) = 25$ meV. Indeed, we also see a very weak feature at about 3.456 eV (not shown), perhaps corresponding to their feature at 3.4547 eV. However, because we see no corresponding DBE ($n=1$) line, we cannot interpret this feature as a TES ($n=2$) line. Instead, it perhaps represents a donor-electron to free-hole transition, with the donor having an energy of about 50 meV. If it indeed exists, this 50-meV donor could arise from complexes formed from the migrating N_i defects. However, we reiterate that neither this possible center, nor the 25-meV center postulated by YFW, have concentrations high enough to be observed by the Hall-effect measurements. In contrast, the 70-meV donor is strongly produced, with a concentration that is close to the theoretically predicted one; thus, only the 70-meV donor is a good

candidate for the isolated N vacancy. In a further comment on PL data in irradiated GaN, we may note that if the dominant O_N DBE line is reduced by pairing with migrating N_i atoms, then the nearby Si_{Ga} DBE line and possibly other weaker DBE lines may appear to be relatively larger, as seen in our PL data (Fig. 2). Depending on spectrometer resolution and other factors, it may be mistakenly assumed that new lines are appearing.

A final argument by YFW is that their 25-meV center is a good candidate for the N vacancy, because this vacancy would be expected to have an energy less than that of O_N , which is known to be nearly hydrogenic with an energy of about 33 – 34 meV.^{7,17} (Note that the ~25-meV donor measured by the Hall effect is equivalent to the ~33-meV donor measured by PL, due to wavefunction overlap and other factors which effectively reduce the Hall energy.⁷) That is, they have suggested that the positive charge of the N vacancy would be distributed over the electron states of the surrounding Ga atoms, and thus the donor electron would require less energy for ionization. However, this simple argument is strongly violated in a very similar case, that of the As vacancy in GaAs. In GaAs, the hydrogenic (0/+) donor energy is about 6 meV, whereas the (0/+) transition of the As vacancy lies at about 140 meV.¹⁸⁻²⁰ Even the (-/0) acceptor transition of the As vacancy, at 45 meV, is deeper than the hydrogenic donor level in GaAs. From this example, the N vacancy in GaN would be expected to be *deeper* than the hydrogenic donor level (as we observe), not *shallower*. However, further consideration of the V_N energy must await accurate theoretical modeling.

1.5 References

1. S.C. Jain, M. Willander, J. Narayan, and R. Van Overstraeten, J. Appl. Phys. **87**, 965 (2000).
2. D.C. Look, phys. stat. sol. (b) **228**, 293 (2001).
3. W.J. Moore, J.A. Freitas, Jr., G.C.B. Braga, R.J. Molnar, S.K. Lee, K.Y. Lee, and I.J. Song, Appl. Phys. Lett. **79**, 2570 (2001).
4. D.C. Look, D.C. Reynolds, J.W. Hemsky, J.R. Sizelove, R.L. Jones, and R.J. Molnar, Phys. Rev. Lett. **79**, 2273 (1997).
5. S.S. Park, I-W. Park, and S.H. Choh, Jpn. J. Appl. Phys., Part 2 **39**, L1141 (2000).
6. D.C. Look and J.R. Sizelove, Appl. Phys. Lett. **79**, 1133 (2001).
7. D.C. Look, J.R. Sizelove, J. Jasinski, Z. Liliental-Weber, K. Saarinen, S.S. Park, and J.H. Han, Mat. Res. Soc. Symp. Proc. **743**, 575 (2003).

8. J. Nord, K. Nordlund, J. Keinonen, and K. Albe, Nucl. Instr. and Meth. in Phys. Res. B **202**, 93 (2003).
9. D.C. Look, *Electrical Characterization of GaAs Materials and Devices* (Wiley, New York, 1989), Ch. 1.
10. J. Nord, private communication.
11. M. Linde, S.J. Uffring, G.D. Watkins, V. Härle, and F. Scholz, Phys. Rev. B **55**, R10177 (1997).
12. K. Saarinen, T. Suski, I. Grzegory, and D.C. Look, Physica B **308-310**, 77 (2001).
13. K.H. Chow, G.D. Watkins, A. Usui, and M. Mizuta, Phys. Rev. Lett. **85**, 2761 (2000).
14. P. Boguslawski, E.L. Briggs, and J. Bernholc, Phys. Rev. B **51**, 17255 (1995).
15. B.K. Meyer, D. Volm, A. Graber, H.C. Alt, T. Detchprohm, A. Amano, and I. Akasaki, Solid State Commun. **95**, 597 (1995).
16. Q. Yang, H. Feick, E.R. Weber, Appl. Phys. Lett. **82**, 3002 (2003).
17. J.A. Freitas Jr., W.J. Moore, B.V. Shanabrook, G.C.B. Braga, S.K. Lee, S.S. Park, J.Y. Han, and D.D. Koleske, J. Cryst. Growth **246**, 307 (2002).
18. D. Pons and J.C. Bourgoin, J. Phys. C **18**, 3839 (1985).
19. B. Ziebro, J.W. Hemsky, and D.C. Look, J. Appl. Phys. **72**, 78 (1992).
20. R. Ambigapathy, A.A. Manuel, P. Hautojärvi, K. Saarinen, and C. Corbel, Phys. Rev. B **50**, 2188 (1994).

Table I. Fitted concentrations and energies for sample S422, irradiated and unirradiated.

Irradiation	N_{D1} (cm ⁻³)	E_{D1} (meV)	N_{D2} (cm ⁻³)	E_{D2} (meV)	N_A (cm ⁻³)
none	1.25×10^{16}	25.9	1.19×10^{15}	72.2	2.30×10^{15}
0.42 MeV	1.07×10^{16}	23.9	8.18×10^{15}	68.5	5.29×10^{15}

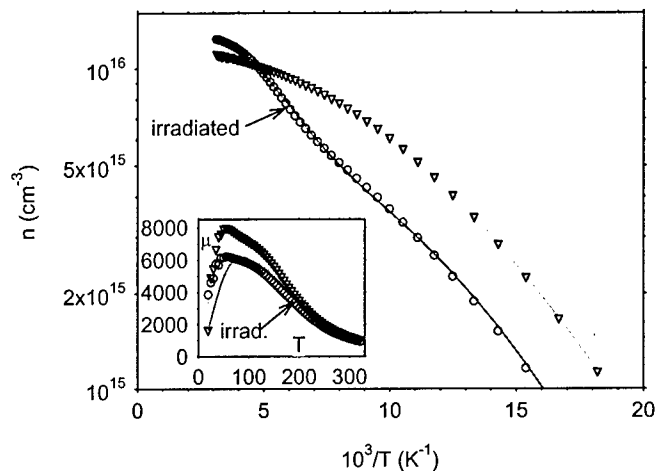


Fig. 1. Carrier concentration, corrected for Hall r-factor, for unirradiated and irradiated sample S422. Inset: Hall mobility, in units of $\text{cm}^2/\text{V}\cdot\text{s}$. All solid lines are theoretical fits to the experimental data (points).

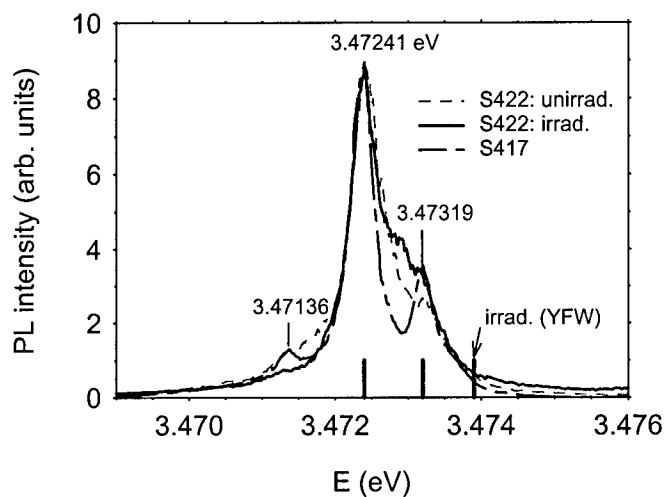


Fig. 2. Photoluminescence donor-bound exciton region for sample S422 (unirradiated and irradiated) and sample S417 (unirradiated). Intensities are normalized to the peak intensity of the 3.47241-eV line. The three, short vertical segments at the bottom of the figure represent lines observed by the authors of Ref. 15 (YFW). The two lowest-energy segments represent PL lines in their unirradiated sample, whereas the highest-energy segment represents a line observed by them only after irradiation.

2.0 Giant traps associated with extended defects in GaN and SiC

2.1 Introduction

It is well-known that impurities and point defects can act as donors, acceptors, recombination centers, and traps in semiconductor materials. For simple point charges, models to describe their effects on electrical and optical properties are readily available. Traps, the subject of this paper, are often investigated by deep level transient spectroscopy (DLTS), and the usual analysis of DLTS data is based on the assumption that each trap has a constant capture cross section, independent of time or the presence of nearby traps [1-3]. Thus, if the Fermi level is suddenly raised, say by applying a forward bias to a Schottky contact, electron traps will capture free electrons in an exponential manner, and if the Fermi level is then returned to its original value, the traps will emit the electrons in the same way. However, large defects, such as dislocations, can often hold many charges, and they are not independent of each other [4-8]. In the case of a threading dislocation, the charges can build up along a line, and gradually begin to repel the accumulation of additional charges. Thus, the effective capture cross section decreases as the accumulated fraction becomes larger, and the capture process is no longer exponential with time. The dynamics of dislocation capture were first elucidated in 1989 [5], and since then have been applied to many experimental situations. Recently, it has been shown that pores also can capture charge [7,8], and that both the capture and emission processes are quite nonexponential [8]. To model this case, a new formalism has been developed [8], and it is applicable to any charge configuration that can be approximated by a sphere, cylinder, or thin slab. Examples of such shapes might include pores, open-core dislocations, and cracks, respectively. In this work, we specifically investigate pores in SiC, and dislocations and microcracks in GaN.

2.2 Theory

Consider a spherical pore of radius r_p with deep, single-level acceptor states of sheet density N_{SS} on its inner surface. If all of the states are filled, then the total number of traps is $4\pi r_p^2 N_{SS}$. However, as more and more electrons are trapped, a negative (repulsive) potential ϕ_{sph} builds up, and the trapping rate diminishes. A spherical region depleted of free electrons, described by a local band bending of *energy* $\Phi_{sph} = -e\phi_{sph}(r_p)$, forms outside the surface ($r = r_p$) of the pore. The value of Φ can be calculated from Poisson's equation, which, for spherical pores, is most conveniently expressed in spherical coordinates:

$$\frac{1}{r^2} \frac{d}{dr} r^2 \frac{d\phi_{sph}}{dr} = -\frac{\rho}{\epsilon} = -\frac{eN_D}{\epsilon} \quad (1)$$

where ρ is the charge density, ϵ is the static dielectric constant, and N_D is the net donor density (actually, $N_D - N_A$, where N_A is the acceptor concentration). By applying charge conservation and the depletion approximation, it can be shown that the *energy*, $\Phi = -e\phi$, is given by

$$\Phi_{sph}(r, f) = \frac{e^2 N_{SS} r_p f}{\epsilon} \left\{ \frac{N_D}{r_p N_{SS} f} \left[\frac{r^2 - r_p^2}{6} \right] + \left[1 + \frac{N_D r_p}{3 N_{SS} f} \right] \left[\frac{r_p}{r} - 1 \right] + 1 + \frac{r_p N_D}{2 N_{SS} f} \left[1 - \left(1 + \frac{3 N_{SS} f}{r_p N_D} \right)^{2/3} \right] \right\} \quad (2)$$

where f is the fractional occupation of the trap states on the pore, i.e., $f = N_{SS}^- / N_{SS}$. Equation 2 holds for $r_p \leq r \leq w$, where w is the depletion length, and is cast in a form which is convenient in that the first two terms drop out for $r = r_p$. (For $r \geq w$, $\Phi = 0$.) For our porous SiC sample, $N_D \approx 10^{18} \text{ cm}^{-3}$ and $r_p \approx 20 \text{ nm}$, and it will turn out that $N_{SS} \approx 2.5 \times 10^{12} \text{ cm}^{-2}$, so that $\Phi(r_p) \approx 0.2 \text{ eV}$, for $f = 1$.

For cylindrical pores, it can be shown that

$$\Phi_{cyl}(r, f) = \frac{e^2 N_{SS} r_p f}{2\epsilon} \left\{ \left[1 + \frac{r_p N_D}{2 N_{SS} f} \right] \left[\ln \left(1 + \frac{2 N_{SS} f}{r_p N_D} \right) - 2 \ln \left(\frac{r}{r_p} \right) \right] + \frac{(r^2 - r_p^2) N_D}{2 r_p N_{SS} f} - 1 \right\} \quad (3)$$

for $r_p \leq r \leq w$. In this case, $\Phi(r_p) \approx 0.3 \text{ eV}$, for $f = 1$.

The dynamic capture and emission processes can now be described by the usual master equation:

$$\frac{df}{dt} = -e_n f + c_n (1 - f) \quad (4)$$

where e_n is the emission rate from filled traps, and c_n is the capture rate into empty traps. Both rates will be affected (slowed down) by the band bending, as follows:

$$c_n(n, T, f) = \sigma v(T) n e^{-\frac{\Phi_{sph}(r_p, f)}{kT}} \equiv c_{n0}(n, T) e^{-\frac{\Phi_{sph}(r_p, f)}{kT}} \quad (5)$$

$$e_n(T, f) = \sigma_{emis} v(T) N_{CB}(T) e^{-\frac{E_{SS0} + \Phi_{sph}(r_p, f)}{kT}} \equiv e_{n0}(T) e^{-\frac{\Phi_{sph}(r_p, f)}{kT}} \quad (6)$$

where $v(T) = (8kT/\pi m^*)^{1/2}$ is the thermal velocity, $N_{CB}(T) = 2(2\pi m^* kT)^{3/2}/h^3$ is the effective conduction band density of states (in the Boltzmann approximation), n is the free electron concentration, σ is the capture cross section for a single trap, and $\sigma_{emis} = (g_0/g_1)\sigma \exp(\alpha/k)$, where g_0 and g_1 are the degeneracies of the unoccupied and occupied trap states, respectively, and α is a linear temperature coefficient: $E_{SS} = E_{SS0}(1 - \alpha T)$. From Eqns. 4 – 6, a general integral equation, describing both capture and emission, can be written for $f(t)$:

$$\int_{f_\alpha}^{f_\beta} \frac{e^{-\frac{\Phi_{sph}(r_p, f)}{kT}}}{1 - f \left[1 + \frac{e_{n0}(T)}{c_{n0}(n, T)} \right]} df = c_{n0}(n, T)(t_\beta - t_\alpha) \quad (7)$$

In a DLTS experiment, the capture process is carried out by applying a forward bias to a normally reversed-biased Schottky barrier or p-n junction [1-3]. In reverse bias, the traps are in a region depleted of free electrons, and thus experience a very low free-electron concentration, $n = n_r \ll n_b$, where n_b is the bulk (neutral) value, 10^{18} cm^{-3} in this case. Thus, $c_{n0}(n_r, T)$ is very small, so that emission dominates and the traps are almost empty. Then, in forward bias, the traps are suddenly exposed to the bulk free-electron concentration $n = n_b$ for a time t_p , the filling pulse length, and at the end of this pulse the filled fraction is defined as f_p . Thus, the trap *filling* process is described by solving Eq. 7 for f_p under the conditions $f_\alpha = 0$, $f_\beta = f_p$, $n = n_b$, $t_\alpha = 0$, and $t_\beta = t_p$. (One convenient means of solving Eq. 7 is by use of the “root” function in Mathcad [9].)

When the filling pulse has ended at time t_p , i.e., by reapplying the reverse bias, the traps are once again suddenly exposed to a very small value of n , i.e., $n = n_r$. (Note that the solution of Eq. 7 is very insensitive to the exact value of n_r , as long as $n_r \ll n_b$.) The traps now emit their carriers, so that the original fractional occupation f_p is now reduced to f_e , in total time $t_p + t_e$. Thus, in *emission*, Eq. 7 is solved for f_e under the conditions $f_\alpha = f_p$, $f_\beta = f_e$, $n = n_r$, $t_\alpha = t_p$, and $t_\beta = t_p + t_e$. In the most common form of DLTS methodology,

used in commercial instruments and often called the “boxcar” technique [1,2], the emission curve is evaluated at two points, t_1 and t_2 (referenced to t_p), and the signal strength is measured as $S \equiv f(t_1) - f(t_2)$. Such a signal is simulated simply by solving Eq. 7 at two times, $t_p + t_1$, and $t_p + t_2$.

To illustrate these ideas, we show in Fig. 1 a band profile along a line perpendicular to the sample surface and cutting through a single, spherical pore, of radius 2 nm, and of depth 22 nm (from the surface). Here the Fermi energy E_F in the bulk (depth $z = \infty$) is set at zero, and in this region E_F is very close to the conduction-band energy E_{CB} , at least for this particular sample. While under reverse bias $V_r = -V$, the surface will be held at energy $e(\phi_B - V_r)$, where ϕ_B is the Schottky-barrier potential, and E_{CB} will vary smoothly from $e(\phi_B - V_r)$ at $z = 0$, to $E_{CB} = 0$ at $z \geq w$, the depletion depth. During the filling pulse, it is assumed (in this case) that $E_{CB} = 0$ all the way to the surface (flat-band approximation), although this assumption is not invoked for the actual calculations. The dashed lines in the figure illustrate the potential barrier formed near the surface of a pore due to the captured charge. This barrier begins to build up as soon as the filling pulse is applied, and then recedes when the filling pulse is removed. The changing barrier energy means that the effective capture and emission rates will change continuously with time, as described by Eq. 7.

Before going on, it is instructive to solve Eq. 7 for a particularly simple case, $\Phi(r_p, f) = 0$ (or a constant), which should hold for isolated point charges. The Eq. 7 yields the usual closed-form, exponential solutions for capture and emission:

$$f_{capt}(T, t_p) = \frac{1}{1 + \frac{e_n(T)}{c_n(n_b, T)}} \left\{ 1 - e^{-[e_n(T) + c_n(n_b, T)]t_p} \right\} \approx \left\{ 1 - e^{-[c_n(n_b, T)]t_p} \right\} \quad (8)$$

$$f_{em}(T, t) = f_{capt}(T, t_p) e^{-[e_n(T) + c_n(n_r, T)](t - t_p)} \square f_{capt}(T, t_p) e^{-e_n(T)(t - t_p)} \quad (9)$$

These equations form the basis of the original DLTS analysis method [1,2], and are still used in the vast majority of cases, as well as in commercial instruments. Besides isolated point charges, line charges have also been considered in the literature [5,6], and the derived *capture* process in this case turns out to be

logarithmic with time. However, such a time dependence is only an approximation, and to derive it from the general formalism, Eq. 7, we must assume (as did Wosinski⁵) the following: (1) small f , such that the denominator of the integrand in Eq. 7 can be approximated by unity; and (2) $\Phi(r_p, f) \propto f$, which means that the large, bracketed terms in Eqns. 2 or 3, respectively, must be independent of f , i.e., a constant K . Then, Eq. 7 yields a logarithmic solution for f (cf. Eq. 3 of Ref. 6), which has been seen experimentally for trapping along dislocation lines[5,6]:

$$f'_{sph}(T, t_p) = \frac{\epsilon k T}{e^2 N_{SS} r_p K_{sph}} \ln \left[1 + \frac{e^2 N_{SS} r_p K_{sph}}{\epsilon k T} c_{n0}(n_b, T) t_p \right] \quad (10)$$

where K_{sph} is typically on the order of 0.1 – 1.

2.3 Pores in SiC

The porous SiC in this study was prepared by photo-assisted electrochemical etching [10] of n-type 6H SiC obtained from Sterling Semiconductor Inc. (now part of Dow-Corning Corp.). The electrolyte was a mixture of HF acid and ethanol. The resistivity of the starting material was about 0.2 Ω -cm, and the carrier concentration $\sim 10^{18}$ cm^{-3} . The C-V and DLTS data were obtained by means of a BioRad DL4600 DLTS apparatus, which operated over the temperature range 80 – 450 K. From the C-V data, the carrier concentration in the nonporous SiC was uniform at about 10^{18} cm^{-3} , whereas that in the porous SiC dropped to about 10^{17} cm^{-3} at a depth of about 80 nm. Cross-sectional transmission electron microscopy (TEM), using a 200kV Phillips CM-200 instrument, was used to study the pore size and density. At depths of 50 – 100 nm below the surface, the pore radii ranged in size from 10 – 25 nm, with a density of about 5×10^{15} cm^{-3} , increasing with depth. The sizes and densities of these pores are very typical of those found at the same depth (just below the so-called “skin layer”) in other P-SiC samples [7,10,11].

In Fig. 2, we compare the capture and emission solutions under three different approximations: (1) exact analysis (Eq. 7); (2) exponential analysis (setting $\Phi_{sph} = 0$, in Eq. 7); and (3) logarithmic analysis (for $f \ll 1$, and $\Phi_{sph} = K e^2 N_{SS} r_p f / \epsilon$ in Eq. 7). To generate the curves, we have used some SiC parameters from the literature: $m^*/m_0 = 0.4$, and $\epsilon/\epsilon_0 = 10$; some parameters measured by TEM or C-V: $r_p = 2 \times 10^{-6}$ cm^{-3} ; $N_D \approx n_b \approx 10^{18}$ cm^{-3} ; and $n_e \approx 10^9$ cm^{-3} (fit not sensitive to n_e); and some fitted parameters (i.e., those needed to fit

the DLTS data of trap T_0 in Fig. 3): $N_{SS} = 2.5 \times 10^{12} \text{ cm}^{-3}$; $E_{SS0} = 0.8 \text{ eV}$; $\sigma = 1 \times 10^{-22} \text{ cm}^2$; and $\sigma_{emis} = 3 \times 10^{-13} \text{ cm}^2$. A filling pulse length $t_p = 20 \text{ ms}$ was assumed for the curves in Fig. 3. The exponential approximation is the one assumed in the vast majority of DLTS experiments, and indeed, it works well for simple, isolated traps such as T_2 (cf. Fig. 3). However, it rises much too fast to explain the capture process of the pore-type traps (T_0 , in Fig. 3). The logarithmic approximation, on the other hand, works fairly well for filling fractions up to about 0.5, but fails beyond that point. From the exact solution, it is seen that even at $t_p = 20 \text{ ms}$, complete saturation has not taken place. Also, in emission, the exact solution is much slower than the exponential solution, because at higher values of f the emitting electrons experience a strong coulomb barrier and are slowed down. In Fig. 2, we have also simulated a boxcar analysis on the BioRad DL4600 instrument by indicating a common set of sampling points, $t_1 = 61.0 \text{ ms}$ and $t_2 = 152.6 \text{ ms}$, referenced with respect to t_p . This choice leads to an emission rate of $\ln(t_2/t_1)/(t_2 - t_1) = 10 \text{ s}^{-1}$ at the signal maximum of a trap such as T_2 (Fig. 3), which has an exponential emission (Eqs. 8 and 9). However, the emission for trap T_0 is far from exponential, so that the “standard” analysis will be highly inaccurate in this case.

The experimental DLTS data, for filling pulse lengths of 0.2, 1.0, 5.0, and 20 ms, are shown as dashed lines in Fig. 3. Here we have plotted $\Delta C/C$, where $\Delta C = C(t_1) - C(t_2)$, and C is the equilibrium capacitance under the reverse-bias condition, $V_r = -5 \text{ V}$. It can be shown that $-\Delta C/C \cong F_\lambda N_T / 2N_D$, where N_T is the trap concentration, and F_λ is a factor which is close to unity for small trap concentrations ($N_T \ll N_D$) and energies that are not too deep, but < 1 otherwise [3]. For our case, $N_T = 4\pi r_p^2 N_{SS} N_p$, where N_p is the volume density of pores. From the TEM measurements, the sheet density of pores is about $3 \times 10^{10} \text{ cm}^{-2}$, and the volume density N_p is then, very approximately, $(3 \times 10^{10})^{3/2} \approx 5 \times 10^{15} \text{ cm}^{-3}$. Thus, $N_T \approx 6 \times 10^{17} \text{ cm}^{-3}$, and from this value and also $E_T = E_{SS} = 0.8 \text{ eV}$, we can calculate $F_\lambda = 0.25$ [3]. The actual DLTS signal is $\propto N_T[f(t_1) - f(t_2)]$, as shown in Fig. 2, and $f(t_1) - f(t_2)$ is calculated to be 0.646 at the peak of the 20-ms theoretical curve, in Fig. 3. Thus, from the TEM data, we would predict that $F_\lambda N_T [f(t_1) - f(t_2)] / N_D \approx 0.10$, whereas we actually need a value of about 0.03 to fit the data at the peak, as shown. In other words, we need an N_T value of about $2 \times 10^{17} \text{ cm}^{-3}$ to fit the data, which is not outside the error of that determined by TEM ($6 \times 10^{17} \text{ cm}^{-3}$), considering that the latter value is a rather crude estimate.

The normalization factor for the 20-ms curve is now applied to the other three theoretical curves, and they reproduce their respective experimental peak magnitudes quite well. Furthermore, the temperature shifts are also well reproduced, giving strong validity to our model. Finally, both the experimental and

theoretical curves become narrower at larger values of t_p . The experimental curves are of course broader than their theoretical counterparts, because we have not considered the known variations in r_p , and the *possible* variations in E_{SS} . The variation in r_p is not likely the cause of the broadening, because neither a doubling nor a halving of the pore size moves the curves by more than a few K. On the other hand, an increase of E_{SS} from 0.80 to 0.85 eV moves the curves up by almost 20 K, which is sufficient to explain the line broadening. Indeed, a ± 0.05 eV variation in E_{SS} seems quite reasonable, since some of the pores will undoubtedly be close enough to influence each other. It also should be noted that adding more traps at different values of E_{SS} would also bring the total, fitted N_T closer to the TEM estimate.

2.4 Microcracks in GaN

Freestanding layers of GaN, grown on Al_2O_3 by hydride vapor phase epitaxy and then separated from the Al_2O_3 , are beginning to be used as substrates for GaN-based devices. Thus, defects in these layers are of both scientific and practical interest. Because these layers are thick, they are subject to cracking, and this problem must be solved before they can become useful. Recently, we have imaged freestanding GaN with scanning surface potential microscopy (SSPM) [12], and have found features that resemble subsurface microcracks, in that they project onto the surface as a straight, narrow strip, of width about $2 \mu m$. The SSPM image of a $40\text{-}\mu m \times 40\text{-}\mu m$ area is shown in Fig. 4, and a line scan of the potential, in Fig. 5. Note that this potential line scan has a shape much like the energy line scan illustrated in Fig. 1 (except inverted). We can attempt to model the microcrack as a thin, infinite-area box with charge on either side, of sheet density N_{SS} . Since charge balance requires that $N_{SS} = N_D w$, and since $w \approx 2 \mu m$, from the figure, and $N_D \approx n \approx 6 \times 10^{15} \text{ cm}^{-3}$, from Hall-effect measurements, we find that $N_{SS} \approx 1 \times 10^{12} \text{ cm}^{-2}$. Then, the potential at the surface should be $\phi \approx eN_{SS}^2/2\epsilon N_D \approx 16 \text{ V}$. This value is, of course, much higher than what is actually measured, possibly because the measurement takes place at the “end” of the box, at the surface, and here the potential may be much reduced from the maximum value, say, that toward the middle of the box. Thus, it’s difficult to be quantitative in this case, but nevertheless, the line scan shown in Fig. 5 clearly is giving information on the lateral shape of the potential around a crack. To be fully understood, this type of problem will have to be explored in more detail.

2.5 Dislocations in GaN

Cherns and coworkers have developed electron holography in conjunction with a transmission electron microscope to study charge on threading dislocations [13,14]. Basically, the interference fringes in the hologram are affected by an electric field in the vicinity of the sample, and this field is of course directly related to the potential. The potential of a cylindrical charge, given by Eq. 3, is directly applicable to an open-core screw dislocation, of radius r_p , with an acceptor sheet density of N_{SS} on the inner surface. However, to model an *edge* dislocation with this formula, we must imagine a small open core of radius r_p , and then define a line charge as $e2\pi r_p N_{SS} L$, where L is the dislocation length. From end-on images of typical threading-edge dislocations in GaN, it seems that a good value for r_p is about 2 Å. The important parameter for comparison with theory and the results of other experiments is the charge per unit length, $e2\pi r_p N_{SS}$. Even more conveniently, it can be normalized to the c-axis parameter, as $e2\pi r_p N_{SS} c$, where $c = 5.185$ Å. Cherns' data (Fig. 3 of Ref. 14) are presented in Fig. 6, and our fit of these data is also shown. For this sample, $N_D \sim 10^{17} \text{ cm}^{-3}$, and the best fit of the potential is then found for $N_{SS} \sim 2.6 \times 10^{14} \text{ cm}^{-2}$, giving a normalized line charge $e2\pi r_p N_{SS} c = 1.7 e$ per c-lattice distance (e/c). Cherns also attempted a fit, but with a much simpler model of the potential, neglecting screening. Nevertheless, his fitted line charge was about $2e/c$, not much different than ours. It should also be mentioned that we have added a positive background potential of 2.6 V in order to fit the data more accurately. It would be interesting to apply a pulsed external potential to this dislocation and study the dynamics of carrier trapping and emission, as was done for the pores in SiC, considered earlier.

2.6 References

- [1] D.V. Lang, J. Appl. Phys. 45, 3023, (1974).
- [2] D.C. Look, *Electrical Characterization of GaAs Materials and Devices* (Wiley, New York, 1989).
- [3] D.C. Look and J.R. Sizelove, J. Appl. Phys. 78, 2848 (1995).
- [4] T. Figielski, Solid-State Electron. 21, 1403 (1978).
- [5] T. Wosinski, J. Appl. Phys. 65, 1566 (1989).
- [6] A. Hierro, A.R. Arehart, B. Heying, M. Hansen, J.S. Speck, U.K. Mishra, S.P. DenBaars, and S.A. Ringel, phys. stat. sol. (b) 228, 309 (2001).
- [7] P. A. Ivanov, M. Mynbaeva and S. E. Saddow, Semicond. Sci. and Tech. 19, 319 (2003).
- [8] D.C. Look, Z-Q. Fang, S. Soloviev, T.S. Sudarshan, and J.J. Boeckl, Phys. Rev. B 69, 195205 (2004).
- [9] Mathsoft, 101 W. Main St., Cambridge, MA 02142

- [10] S. Soloviev, T. Das, and T.S. Sudarshan, *Electrochem. and Sol. State Lett.* **6**, G22 (2003).
- [11] A. Sagar, C.D. Lee, R.M. Feenstra, C.K. Inoki, and T.S. Kuan, *J. Appl. Phys.* **92**, 4070 (2002).
- [12] A. Krtshil, A. Dadgar, and A. Krost, *J. Cryst. Growth* **248**, 529 (2003).
- [13] D. Cherns and C.G. Jiao, *Phys. Rev. Lett.* **87**, 5504 (2001).
- [14] D. Cherns, C.G. Jiao, H. Mokhtari, J. Cai, and F.A. Ponce, *phys. stat. sol. (b)* **234**, 924 (2002).

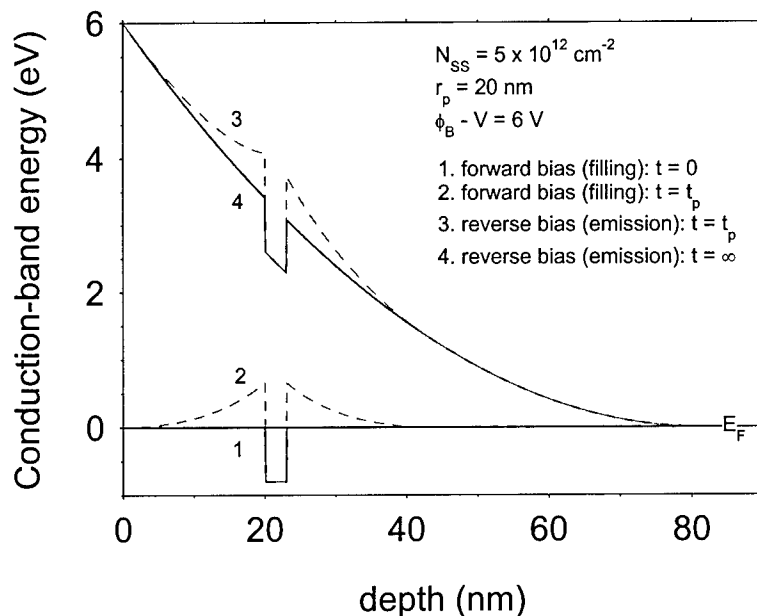


Fig. 1 Conduction band profiles under reverse bias, and forward bias, respectively. The dashed lines denote the bands after the filling pulse (curve 2, at the end of the filling pulse but still in forward bias; and curve 3, immediately after reapplication of the reverse bias).

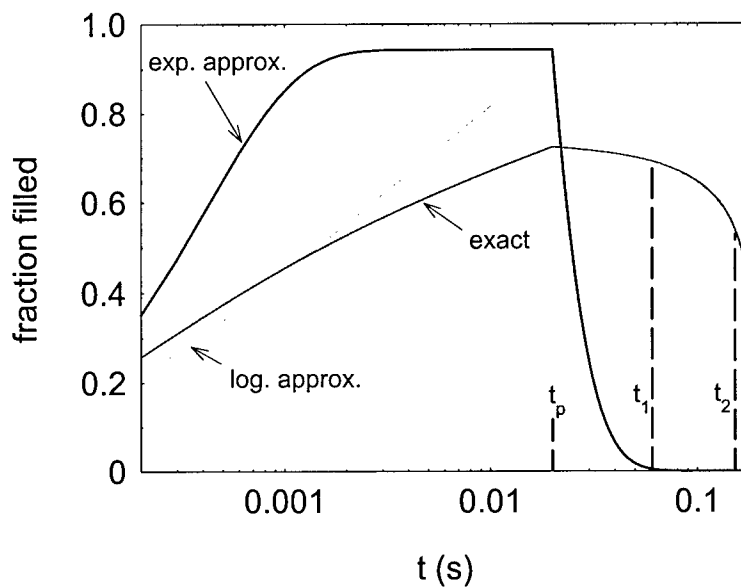


Fig. 2 Fractional occupation, during capture and emission at 350 K, of a pore in porous SiC. An exact calculation is compared with exponential and logarithmic approximations. The filling pulse length is t_p , and the sampling points on the emission transient are t_1 and t_2 , respectively.

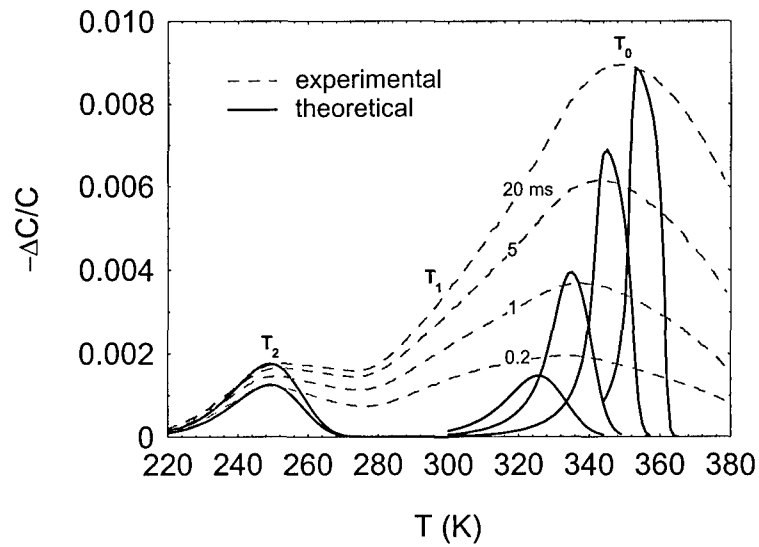


Fig. 3 Experimental (dashed lines) and theoretical (solid lines) DLTS curves for different filling-pulse lengths, 0.2, 2, 5, and 20 ms, in porous SiC. Trap T_2 is a “normal” trap (impurity or point defect), which obeys exponential kinetics, and trap T_0 is related to the pores.

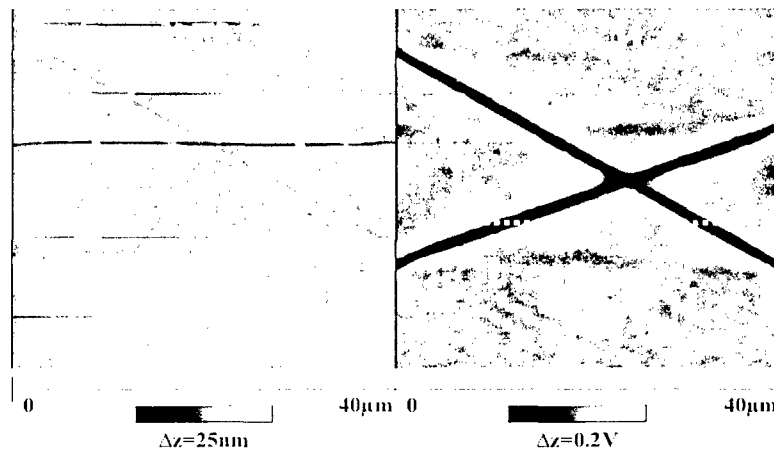


Fig. 4 AFM and SSPM images of microcrack-like defects in HVPE GaN. A line scan of the surface potential, shown in Fig. 5, has a path denoted by the dotted line in this figure.

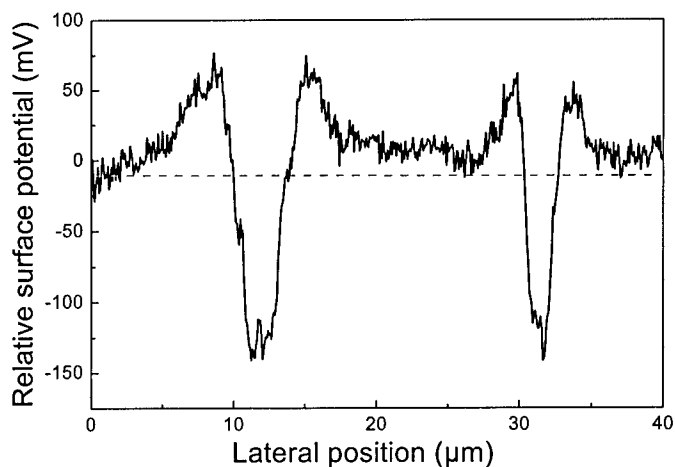


Fig. 5 Lateral profile of the surface potential along the dotted line shown in Fig. 4. Note that the line crosses two cracks.

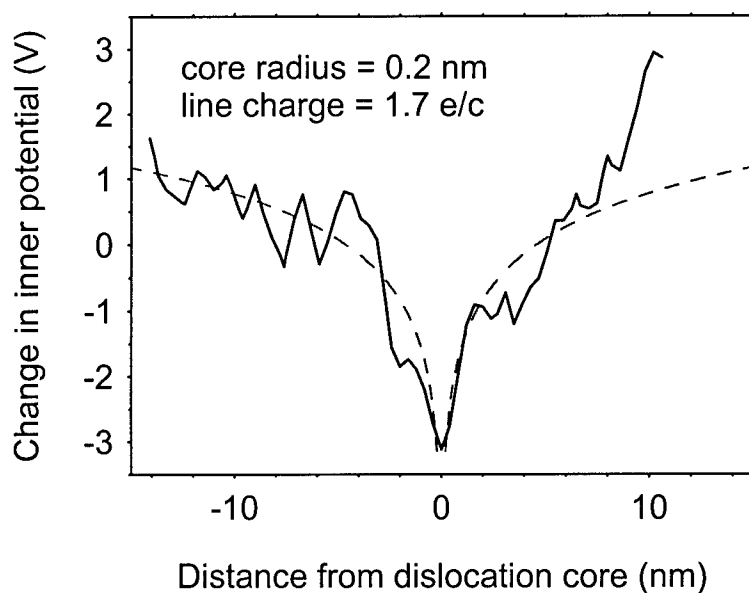


Fig. 6 Lateral potential profile across a threading-edge dislocation in GaN. The dotted line is a theoretical fit, assuming a line charge of 1.7 e/c.

3.0 Characterization of bulk-like GaN grown by hydride vapor phase epitaxy

3.1 Introduction

GaN grown by hydride vapor phase epitaxy (HVPE) has a high growth rate ($\sim 100 \mu\text{m}$ per hr), and thus is capable of growing thick material, more than $1000 \mu\text{m}$ in some cases [1-5]. Although these layers are usually grown on Al_2O_3 substrates, they can be easily separated from the Al_2O_3 by a laser irradiation technique [4]. Recently, separated (or unseparated) HVPE wafers have been proposed as a solution to the GaN substrate problem because, unlike the cases in Si, GaAs, SiC, and ZnO, large-area wafers of GaN cannot be obtained by the usual bulk-growth techniques. Thus, it is important to characterize the electrical properties of these HVPE GaN templates, and, in particular, to identify and determine the concentrations of their dominant donors, acceptors, and traps. It is well known that HVPE GaN layers grown on Al_2O_3 can often be described in terms of two regions, a highly conductive layer adjacent to the GaN/ Al_2O_3 interface, of thickness $0.2 - 50 \mu\text{m}$, and the rest of the sample, comprising the "bulk" portion, of much lower conductivity [6]. The interface layer has been extensively studied in the past, and contains very high concentrations of O_N donors and Ga-vacancy acceptors, as shown in Fig. 1, and also threading dislocations [7-10]. However, thick layers usually have a strong bow after growth, and have to be ground flat before being used as substrates for subsequent growth of an active layer [3,4]. This grinding/polishing process typically removes all or part of the low-quality interface layer so that only the higher-quality bulk region remains. We would normally like the bulk region to be as pure as possible in order to avoid diffusion of impurities and defects into the active layer and the trapping of carriers injected from the active layer into the substrate. It is the purpose of this work to review our present knowledge of donors, acceptors, and traps in thick HVPE GaN and present some new results and interpretations. We will deal principally with HVPE GaN layers grown at three different laboratories, designated as A, B, and C. Lab-A and Lab-C samples are $1\text{-}\mu\text{m}$ and $30\text{-}\mu\text{m}$ thick, respectively, and are still on their Al_2O_3 substrates. The Lab-B sample, on the other hand, was originally $500\text{-}\mu\text{m}$ thick, and then was separated from its Al_2O_3 substrate and ground and polished flat to a thickness of $250 \mu\text{m}$.

3.2 Secondary ion mass spectroscopy: donor-type impurities

Secondary-ion mass spectroscopy (SIMS) measurements [10] of [Si], [O], and [C] have been carried out on the Lab-A and Lab-B samples. In the bulk regions, both samples show [O] and [C] in the mid 10^{16}

cm⁻³ range, but the Lab-A sample has [Si] > [O] in this region (see Fig. 1), and the Lab-B sample, [O] > [Si]. Another group has carried out SIMS measurements on material from Lab B, and has also found that [O] > [Si]. From temperature-dependent Hall-effect (T-Hall) measurements, discussed below, we find that the total shallow donor concentration in the Lab-B sample is only about 8×10^{15} cm⁻³, a lower value than [O] + [Si], as determined by SIMS. However, SIMS measurements are not always accurate at these low concentrations, and, also, some of the O and Si may not be electrically active as donors. The other common impurity, C, would be expected to substitute for N and be an acceptor in n-type GaN, but the SIMS value of [C], mid- 10^{16} cm⁻³, is much greater than the acceptor concentration N_A , low- 10^{15} cm⁻³, determined by the Hall effect; thus, either the SIMS data are not accurate due to background limitations, or most of the C is not electrically active. In this regard, it should be pointed out that the profiles of C and O in some of these samples are quite similar, suggesting a correlation between the two, either in the sample or the background.

3.3 Positron annihilation spectroscopy (PAS): acceptor-type defects

Positrons injected into defect-free GaN are annihilated by electrons in a mean time of 160 – 165 ps. However, if there are negatively charged vacancies present, some of the positrons will become trapped at these locations, and will have longer lifetimes, because of the reduced electron density at vacancies. In the case of GaN, the Ga vacancy V_{Ga} (but not the N vacancy) would be expected to fill this role, and indeed, PAS has been used to identify and quantify V_{Ga} -related defects [9]. In fact, comparisons of V_{Ga} concentrations with acceptor concentrations N_A in a series of Lab-A HVPE GaN samples, with N_A ranging from 10^{15} to 10^{19} cm⁻³, show that $[V_{Ga}] \approx N_A$, to within experimental error [7,9]. Also, a sample from Lab B has been shown to have $[V_{Ga}] \approx 2 \times 10^{15}$ cm⁻³ [9], very close to our value of N_A determined by T-Hall measurements, discussed below. Thus, it appears that V_{Ga} , and not any impurity, is the dominant acceptor in HVPE GaN. Indeed, theory predicts that V_{Ga} centers should be abundant in n-type GaN [11]. However, in GaN grown by some other techniques, such as by low-pressure metal-organic vapor-phase epitaxy, the dominant acceptor is C_N , rather than V_{Ga} .

3.4 Photoluminescence - donors

A 4-K PL spectrum of the near-band-edge (exciton) region, 3.43 – 3.48 eV, is shown in Fig. 2 for a HVPE GaN sample from Lab B. The sharp lines at 3.47123, 3.47225, and 3.47305 eV are likely neutral donor-bound A excitons (D^0X_A 's), while the broader line at 3.4792 eV is the free A exciton X_A . The line at

3.47609 eV may be an excited (rotator) state of a D^0X_A species, or possibly a D^0X_B transition. It has been reported that the D^0X_A line in *unstrained* material should lie at 3.471 - 3.472 eV, a result that suggests immediately that the present Lab-B sample does not have a high strain. This is expected, since strain decreases with thickness, and this sample is 250- μm thick. The full width at half maximum (FWHM) for each of these D^0X lines is about 0.4 meV, which indicates excellent quality. Another group of PL lines appears in the region 3.44 - 3.46 eV, with a strong line at 3.44686 eV and a somewhat weaker one at a slightly higher energy, 3.44792 eV. Most workers agree that the 3.44686-eV line is a two-electron satellite (TES) replica of one of the three D^0X transitions, although there is disagreement over which one. The 3.44792-eV line would then be a TES transition from an excited (rotator) state of that particular D^0X line. However, there are also a few weaker lines at even lower energies, and two of these are designated $n=3$ and $n=4$ in Fig. 2. We have earlier pointed out [12] that if we combine these two lines with the strongest $n=1$ D^0X line at 3.47225 eV, and the strongest $n=2$ line at 3.44686, then, as seen in the inset of Fig. 2, all four peak energies closely follow the hydrogenic relationship, $E_{PL,n} = E_{PL,1} - R_{\text{expt}}(1 - 1/n^2) = 3.47225 - 0.0339(1-1/n^2)$, so that $R_{\text{expt}} = 33.9$ meV. R_{expt} is the “experimental” Rydberg for GaN. The theoretical Rydberg is derived from effective-mass theory: $R_{\text{theo}} = 13.6m^*/\epsilon_0^2$ eV, where m^* is the electron effective mass relative to the rest mass, and ϵ_0 is the dielectric constant relative to the value in vacuum. The presently accepted values of m^* and ϵ_0 are 0.22 [13] and 9.4 [14], respectively, giving $R_{\text{theo}} = 33.9$ meV, fortuitously close to R_{expt} . The clear and simple interpretation of these results is that the donor represented by the D^0X line at 3.47225 eV is truly hydrogenic, i.e., effective-mass-like. From the SIMS results, the two obvious candidates for this donor are Si_{Ga} and O_{N} ; however, it would seem that O_{N} is by far the better of the two candidates, because O and N have nearly equal ionic radii, and thus only a small lattice distortion would be expected from the replacement of N with O. In other words, the potential in the vicinity of O_{N} should be just that of the original N_{N} plus a point positive charge at the core, which should lead to a hydrogen-like potential. Interestingly, a recent calculation based on effective-mass theory [15] shows that the details of the band-edge wave function don't make much difference for the O_{N} donor energy, whereas they do for the energies of other donors, such as Si_{Ga} . This fact would seem to support the idea that O_{N} is hydrogenic or nearly so. In this same paper, the hydrogenic ground state energy (Rydberg) was given as $R_{\text{theo}} = 29.6$ meV; that number was evidently derived from the usual formula $(13.6m^*/\epsilon_0^2)$, but with older values of dielectric constant $\epsilon_0 = 9.8$, and effective masses $m_{\parallel} = 0.19$ and $m_{\perp} = 0.22$ [giving an average $m^* = (m_{\parallel} m_{\perp}^2)^{1/3} = 0.209$]. Our values of $m^* = 0.22$ and $\epsilon_0 = 9.4$ both come from recent experiments, and thus our value $R_{\text{theo}} =$

33.9 meV may be more accurate. In any case, the origin of the difference between the values 29.6 and 33.9 meV is well understood. Another disagreement, however, which is not understood, involves a comparison of 2p and 3p IR-absorption states [13], which leads to an experimental value of the Rydberg, $R_{\text{expt}} = 29.1 \pm 0.5$ meV, much smaller than our value, $R_{\text{expt}} = 33.9$ meV. This difference will require further investigation.

Another controversial issue is concerned with the identification of the dominant D⁰X line at 3.47225 eV. It was originally identified as O_N rather than Si_{Ga} mainly on the basis of SIMS data, i.e., because these data show more O than Si in nearly all samples from Lab B [16]. However, as mentioned earlier, a SIMS measurement of a particular element, say O, includes all of that element, not just the substitutional fraction (O_N in this case). In this regard, we note that the SIMS values of [O] and [Si] in Lab-B samples are always significantly higher than the *total* donor concentration, as measured by T-Hall measurements. Thus, SIMS measurements are not conclusive here. To further complicate the O-vs.-Si matter, another group [17] has compared the transient behaviors of the 3.47225-eV (n=1) and 3.44686-eV (n=2) lines, and has concluded that these lines cannot have a common origin. Instead, they associate the 3.47123-eV (n=1) line with the 3.44686-eV (n=2) line, and assign both to O_N. But a brief glance at Fig. 2 illustrates a potential problem with this assignment, namely that the 3.47123-eV (n=1) line is by far the weakest D⁰X line, and the 3.44686-eV (n=2) line, by far the strongest TES line. In the present work, we are suggesting that the 3.47225-eV (n=1), 3.44686-eV (n=2), 3.44215-eV (n=3), and 3.44051-eV (n=4) lines all belong to O_N, not on the basis of SIMS or transient PL, but because these four lines seem to fit a 33.9-meV hydrogenic model very well, and that the best candidate for a hydrogenic donor is O_N, rather than Si_{Ga}. However, at this point, we cannot explain the experimental Rydberg of 29.1 meV, derived from the 2p and 3p absorption lines [13], or the difference in transient PL behavior of the 3.47225-eV (n=1) and 3.44686-eV (n=2) PL lines [17]. Clearly, more work needs to be done to clear up these matters.

3.5 Hall-effect measurements: donors and acceptors

In a simple picture, conductivity is defined by $\sigma = ne\mu_c$, where n is the carrier (electron) concentration (not to be confused with the symbol for quantum number, used previously), and μ_c is the conductivity mobility, defined by $\mu_c = e\langle\tau\rangle/m^*$. Here, τ is a “relaxation time”, obeying [18]

$$\tau^{-1}(E) = \tau_{\text{ac}}^{-1}(E) + \tau_{\text{pe}}^{-1}(E) + \tau_{\text{po}}^{-1}(E) + \tau_{\text{ii}}^{-1}(E) + \tau_{\text{dis}}^{-1}(E) \quad (1)$$

and $\langle\tau\rangle$ denotes an average over energy E . The relaxation time, $\tau(E)$, depends upon how the electrons interact with the lattice vibrations as well as with extrinsic elements, such as charged impurities and defects. For example, acoustical-mode lattice vibrations scatter electrons through the deformation potential (τ_{ac}) and piezoelectric potential (τ_{pe}); optical-mode vibrations through the polar potential (τ_{po}); ionized impurities and defects through the screened coulomb potential (τ_{ii}); and charged dislocations, also through the coulomb potential (τ_{dis}). The strengths of these various scattering mechanisms depend upon certain lattice parameters, such as dielectric constants and deformation potentials, and extrinsic factors, such as donor, acceptor, and dislocation concentrations, N_D , N_A , and N_{dis} , respectively [18-20]. In reality, a closed-form expression for τ_{po} cannot be written, but suitable approximations are available [21].

In general, it is difficult to measure μ_c , but much easier to measure $\mu_H = R_H\sigma$, where R_H is the Hall coefficient. In the relaxation-time approximation, μ_H is calculated from $\mu_H = e\langle\tau^2\rangle/m^*\langle\tau\rangle = r\mu_c$. It is also convenient to define a "Hall concentration", $n_H = n/r = -1/eR_H$. Thus, a combined Hall-effect and conductivity measurement gives n_H and μ_H , although we would prefer to know n , not n_H ; fortunately, however, r is usually within 20% of unity, and is almost never as large as two. In any case, r can often be calculated or measured so that an accurate value of n can usually be determined.

The fitting of μ_H vs. T data should be carried out in conjunction with the fitting of n vs. T data, and the relevant expression here is the charge-balance equation [18]:

$$n + N_A = \frac{N_D}{1 + n/\phi_D} \quad (2)$$

where we have assumed only one type of donor, with a single charge state, and where

$$\phi_D = \frac{g_0}{g_1} e^{\frac{\alpha_D}{k}} N_C' T^{3/2} e^{-\frac{E_{D0}}{kT}} \quad (3)$$

Here, g_0/g_1 is a degeneracy factor, $N_C' = 2(2\pi m_n^*k)^{3/2}/h^3$ is the effective conduction-band density of states at 1K, h is Planck's constant, E_D is the donor ground-state energy, and E_{D0} and α_D are defined by $E_D = E_{D0} - \alpha_D T$. If more than one donor is needed to fit the data, then equivalent terms are added on the right hand side of Eq. 2. As mentioned earlier, examples of common, single-charge-state donors in GaN are Si_{Ga} and O_N . If there are double or triple donors, or more than one acceptor, proper variations of Eq. 2 can be found in the literature [18].

If the donors are effective-mass-like, they will have a set of excited states, much like those of hydrogen. Using standard statistical theory, we can add hydrogenic-type excited states ($j = 2, 3, \dots, m$) to the analysis by modifying ϕ_D [18,22].

$$\phi_D = \frac{g_0}{g_1} e^{\frac{\alpha_D}{k}} N_C T^{3/2} \frac{e^{-\frac{E_{D0}}{kT}}}{1 + \sum_{j=2}^m j^2 e^{-\left(1 - \frac{1}{j^2}\right) \frac{E_{D0}}{kT}}} \quad (4)$$

where we have assumed that $g_j/g_0 = j^2$, as is the case for the hydrogen atom, and also that α_D is the same for each state. (Actually, in any case, α_D should be small for an effective-mass-like donor state.) At low temperatures, only the ground state will be occupied, and the additional term in the denominator of Eq. 4 will be small. However, at higher temperatures, the n vs. T curve will be modified [12].

The Lab-B Hall mobility μ_H data, and the theoretical fit are plotted vs. temperature in Fig. 3. From these data, an acceptor concentration $N_A = 1.3 \times 10^{15} \text{ cm}^{-3}$ is deduced, the lowest ever determined in GaN. The carrier concentration data, corrected for the Hall r -factor, are plotted in Fig. 4, along with the theoretical fit (Eq. 2). Here two donors are found from the fit: $N_{D1} = 7.8 \times 10^{15} \text{ cm}^{-3}$, $E_{D1} = 28.1 \text{ meV}$; and $N_{D2} = 1.1 \times 10^{15} \text{ cm}^{-3}$, $E_{D2} = 53.2 \text{ meV}$. Also, the fitted acceptor concentration N_A is $7.2 \times 10^{14} \text{ cm}^{-3}$, a little smaller than the value found from the mobility fit, but not considered to be as accurate as the latter. Note that $E_D(\text{Hall}) < E_D(\text{PL})$ by a few meV, as is expected from the effects of wavefunction overlap and excited donor states, as discussed in detail elsewhere [12].

The most straightforward interpretation of all of the above results, is that the Lab-B sample contains O_N at a concentration of $8 \times 10^{15} \text{ cm}^{-3}$, and that O_N forms a hydrogenic donor of energy 33.9 meV from the conduction band, with distinctive PL lines and a Hall-effect energy a little smaller, 28.1 meV, in this particular case.

3.6 References

1. H.P. Maruska and J.J. Tietjen, *Appl. Phys. Lett.* **15**, 327 (1969).
2. R.J. Molnar, K.B. Nichols, P. Makai, E.R. Brown, and I. Melngailis, *Mater. Res. Soc. Symp. Proc.* **378**, 479 (1995).
3. S.S. Park, I-W. Park, and S.H. Choh, *Jpn. J. Appl. Phys., Part 2* **39**, L1141 (2000).

4. E. Oh, S.K. Lee, S.S. Park, K.Y. Lee, I.J. Song, and J.Y. Han, *Appl. Phys. Lett.* **78**, 273 (2001).
5. G.A. Smith, T.N. Dang, T.R. Nelson, J.L. Brown, D. Tsvetkov, A. Usikov, and V. Dmitriev, *J. Appl. Phys.* **95**, 8247 (2004).
6. D.C. Look and R.J. Molnar. *Appl. Phys. Lett.* **70**, 3377 (1997).
7. D.C. Look, C.E. Stutz, R.J. Molnar, K. Saarinen, and Z. Liliental-Weber, *Solid State Commun.* **117**, 571 (2001).
8. J. Jasinski and Z. Liliental-Weber, *J. Electron. Mater.* **31**, 429 (2002).
9. J. Oila, J. Kivioja, V. Ranki, K. Saarinen, D.C. Look, R.J. Molnar, and S.S. Park, *Appl. Phys. Lett.* **82**, 3433 (2003).
10. Evans East, 104 Windsor Center, East Windsor, NJ, 08520
11. J. Neugebauer and C.G. Van de Walle, *Phys. Rev. B* **50**, 8067 (1994).
12. D.C. Look, J.R. Sizelove, J. Jasinski, Z. Liliental-Weber, K. Saarinen, S.S. Park, and J.H. Han, *Mat. Res. Soc. Symp. Proc.* **743**, 575 (2003).
13. W.J. Moore, J.A. Freitas, Jr., S.K. Lee, S.S. Park, and J.Y. Han, *Phys. Rev. B* **65**, 081201 (2002).
14. W. Zhang, A.K. Azad, and D. Grischkowsky, *Appl. Phys. Lett.* **82**, 2841 (2003).
15. H. Wang and A.-B. Chen, *J. Appl. Phys.* **87**, 7859 (2000).
16. J.A. Freitas, Jr., W.J. Moore, B.V. Shanabrook, G.C.B. Braga, D.D. Koleske, S.K. Lee, S.S. Park, and J.Y. Han, *phys. stat. sol. (b)* **240**, 330 (2003).
17. A. Wyszomolek, K.P. Korona, R. Stępniewski, J.M. Baranowski, J. Bloniarz, M. Potemski, R.L. Jones, D.C. Look, J. Kuhl, S.S. Park, and S.K. Lee, *Phys. Rev. B* **66**, 245317 (2002).
18. D.C. Look, *Electrical Characterization of GaAs Materials and Devices* (Wiley, New York, 1989), Ch.1.
19. D.L. Rode, *Semicond. Semimetals* **10**,1 (1975).
20. B.R. Nag, *Electron Transport in Compound Semiconductors* (Springer, Berlin, 1980).
21. D.C. Look, "Hall Effect in Semiconductors", in *Methods in Materials Research*, ed. by A.C. Samuels (Wiley, New York, 2000), p. 5a.2.1.
22. D.V. Eddolls, J.R. Knight, and B.L.H. Wilson, in *Proc. Int. Symp. on GaAs*, ed. by J. Franks and W.G. Moore (Inst. Phys., London, 1967) pp.3-9.

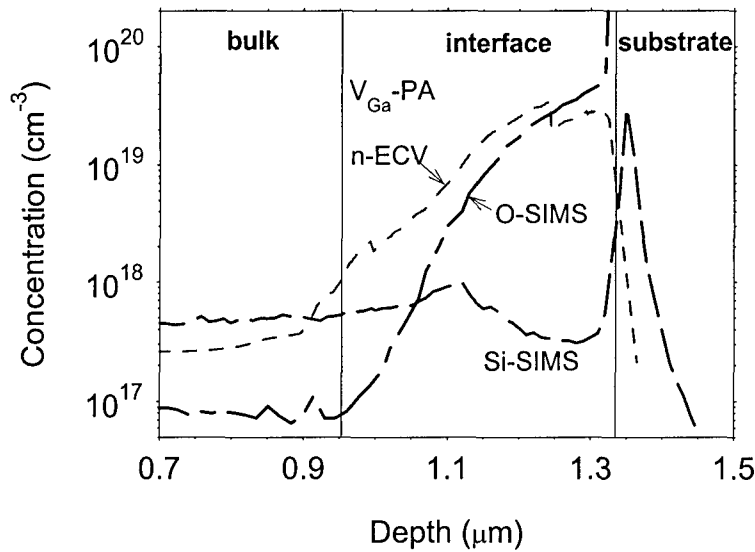


Fig. 1. The interface region of a 1.3-μm-thick Lab-A HVPE GaN layer grown on an Al₂O₃ substrate. Shown are SIMS profiles for O and Si, an electrochemical C-V profile for the electron concentration n , and the average Ga-vacancy V_{Ga} concentration deduced from positron annihilation spectroscopy.

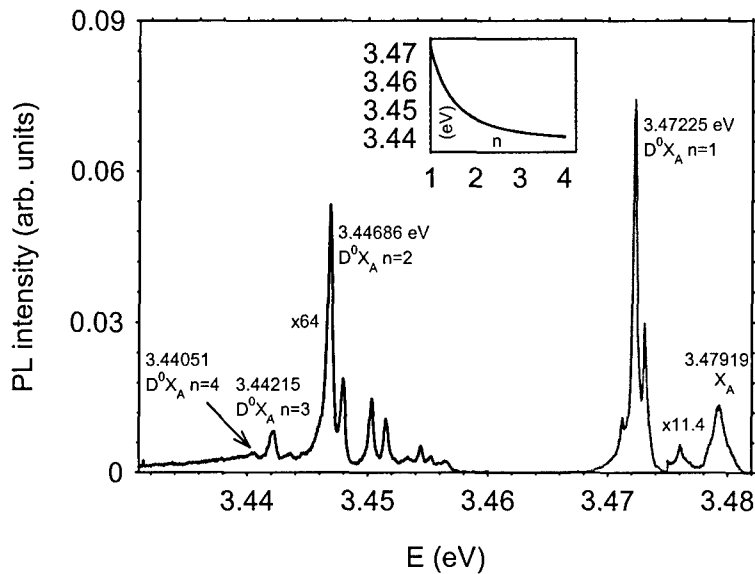


Fig. 2. Photoluminescence spectrum in the donor-bound-exciton (D⁰X) and two-electron satellite regions. The four lines marked D⁰X $n=1$, etc, have been plotted in the inset and obey the relationship $E_{\text{PL},n} = 3.47225 - 0.0339(1-1/n^2)$.

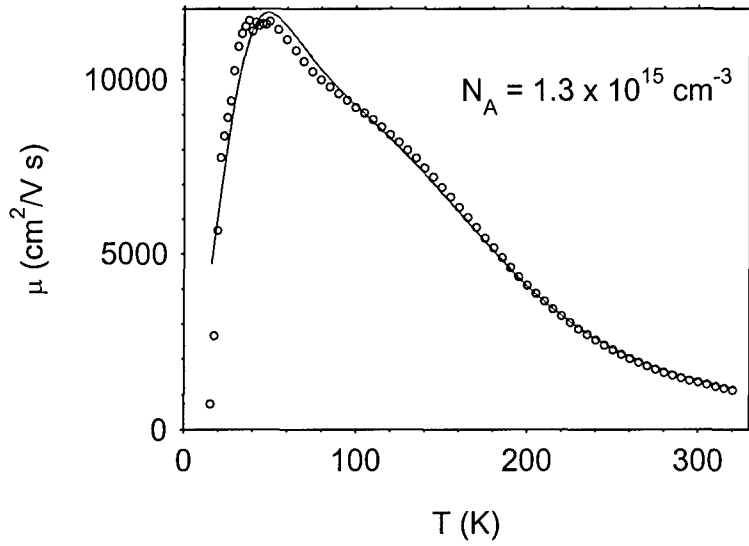


Fig. 3. Mobility vs. temperature for a Lab-B HVPE GaN layer. The solid line is a theoretical fit.

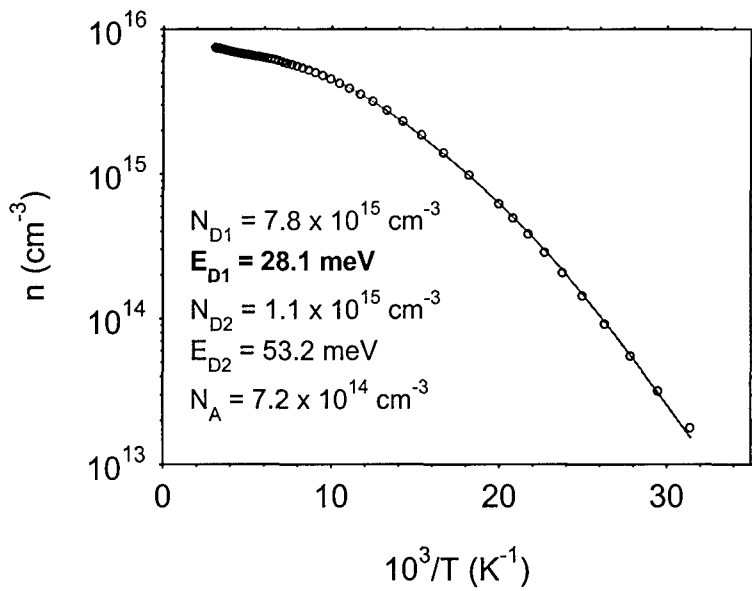


Fig. 4. Carrier concentration vs. inverse temperature for a Lab-B HVPE GaN layer. The solid line is a theoretical fit.

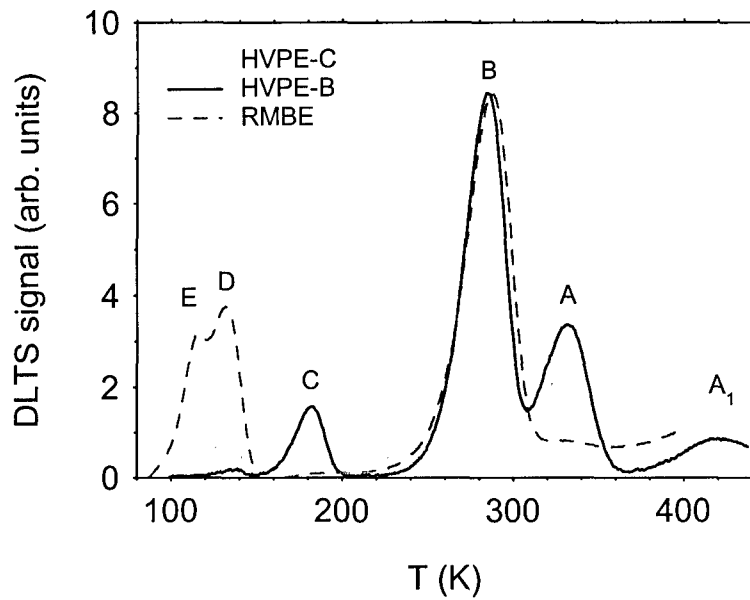


Fig. 5. A comparison of DLTS data for two HVPE samples, and an RMBE sample.

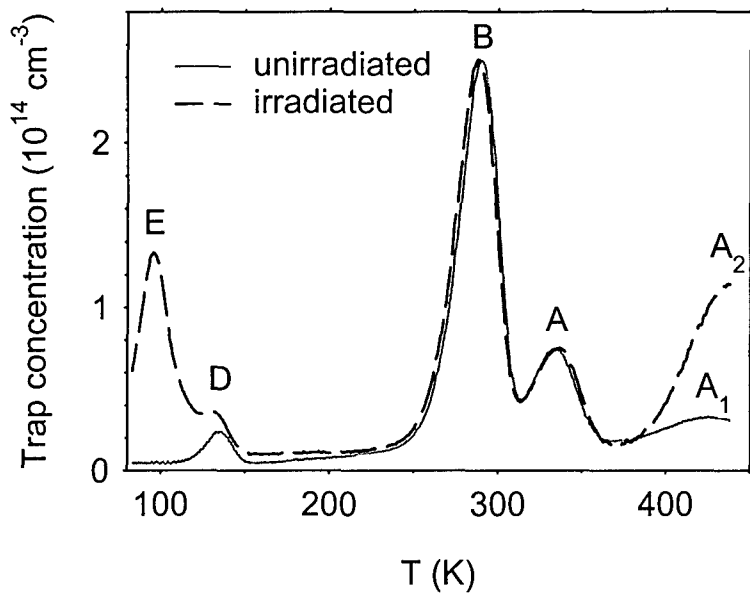


Fig. 6. Effects of electron irradiation (1 MeV , $1 \times 10^{16} \text{ cm}^{-2}$) on HVPE-C GaN/ Al_2O_3 layer.

4.0 List of Publications

1. D.C. Reynolds, J. Hoelscher, C.W. Litton, T.C. Collins, R. Fitch, G.D. Via, J. Gillespie, A. Crespo, T.J. Jenkins and A. Saxler, "Emission and reflection spectra from $\text{Al}_x\text{Ga}_{1-x}\text{N}/\text{GaN}$ single heterostructures", *J. Appl. Phys.* **94**, 4263 (2003).
2. A. Wysmolek, M. Potemski, R. Stepniewski, J.M. Baranowski, R.L. Jones, D.C. Look, S.K. Lee, and J.H. Han "Resonant interaction of LO phonons with excited donor states in GaN", *phys. stat. sol. (b)* **235**, 36 (2003).
3. D.C. Look, J.R. Sizelove, J. Jasinski, Z. Liliental-Weber, K. Saarinen, S.S. Park, and J.H. Han, "Electrical, Optical, Structural, and Analytical Properties of Very Pure GaN", *Mat. Res. Soc. Symp. Proc.* **743**, 575 (2003).
4. J. Oila, J. Kivioja, V. Ranki, K. Saarinen, D.C. Look, R.J. Molnar, S.S. Park, S.K. Lee, and J.Y. Han, "Ga vacancies as dominant acceptors in GaN grown by hydride vapor phase epitaxy", *Appl. Phys. Lett.* **82**, 3433 (2003).
5. Z-Q. Fang, B.B. Claflin, D.C. Look, T.H. Myers, D.D. Koleske, A.E. Wickenden, and R.L. Henry, "High-Temperature Illumination-Induced Metastability in Undoped Semi-Insulating GaN Grown by Metalorganic Vapor Phase Epitaxy", *Mat. Res. Soc. Symp. Proc.* **743**, 749 (2003).
6. M. Pavlović, U.V. Desnica, Z.-Q. Fang, and D.C. Look, "Thermoelectric effect spectroscopy measurements on semi-insulating GaN", *Vacuum* **71**, 153 (2003).
7. C. Coşkun, D.C. Look, G.C. Farlow, and Z.-Q. Fang, "Experimental set-up for *in-situ* Hall measurements under high-energy electron irradiation for wide-bandgap materials", *Meas. Sci. Technol.* **15**, 297 (2003).
8. Z-Q. Fang, D.C. Look, X-L. Wang, J. Han, F.A. Khan, and I. Adesida, "Plasma-etching-enhanced deep centers in n-GaN grown by metalorganic chemical-vapor deposition", *Appl. Phys. Lett.* **82**, 1562 (2003).
9. X.L. Sun, S.T. Bradley, G.H. Jessen, D.C. Look, R.J. Molnar, and L.J. Brillson, "Micro-Auger electron spectroscopy studies of chemical and electronic effects at GaN-sapphire interfaces", *J. Vac. Sci. Technol. A* **22**, 2284 (2004).
10. M.J. Yannuzzi, N.A. Moser, R.C. Fitch, G.H. Jessen, J.K. Gillespie, G.D. Via, A. Crespo, T.J. Jenkins, D.C. Look, and D.C. Reynolds "Effects of Pre-Process Temperature Stressing on AlGaIn/GaN HEMT Structures", *Mat. Res. Soc. Symp. Proc.* **764**, C4.2.1 (2003).
11. D.C. Look, G.C. Farlow, P.J. Drevinsky, D.F. Bliss, and J.R. Sizelove, "On the nitrogen vacancy in GaN", *Appl. Phys. Lett.* **83**, 3525 (2003).

12. P.W. Yu, J.D. Clark, D.C. Look, C.Q. Chen, J.W. Yang, E. Koutstis, M.A. Khan, D.V. Tsvetkov, and V.A. Dmitriev, "Below bandgap photorefectance transitions in epitaxial GaN", *Appl. Phys. Lett.* **85**, 1931 (2004).
13. K.P. Korona, A. Wyszomolek, R. Stepniowski, J. Kuhl, D.C. Look, S.K. Lee, and J.Y. Han, "Dynamics of Ground and Excited States of Bound Excitons in GaN", *J. Lumin.* **112**, 30 (2005).
14. Z-Q. Fang, D.C. Look, R. Armitage, Q. Yang, and E.R. Weber, "Thermally stimulated current spectroscopy of carbon-doped GaN grown by molecular beam epitaxy", *Mat. Res. Soc. Symp. Proc.* **798**, 521 (2004).
15. C.H. Swartz, R.P. Tompkins, T.H. Myers, D.C. Look, and J.R. Sizelove, "Characterization of Multiple Carriers in GaN Using Variable Magnetic-Field Hall Measurements", *J. Electronic. Mater.* **33**, 412 (2004).
16. Z-Q. Fang, D.C. Look, B. Claflin, S. Haffouz, H. Tang, and J. Webb, "Thermally stimulated current spectroscopy and photoluminescence of carbon-doped semi-insulating GaN grown by ammonia-based molecular beam epitaxy", *phys. stat. sol. (c)* **2**, 2757 (2005).
17. D.C. Look, Z-Q. Fang, and B. Claflin, "Identification of donors, acceptors, and traps in bulk-like HVPE GaN", *J. Crystal Growth* **281**, 143 (2005).
18. D.C. Look, Z-Q. Fang, A. Krtschil, A. Krost, "Giant traps associated with extended defects in GaN and SiC", *phys. stat. sol. (c)* **2**, 1039 (2005).
19. Z-Q. Fang, G. Farlow, B. Claflin, and D.C. Look, "Deep Centers in Conductive and Semi-insulating GaN", in *2004 13th International Conference on Semiconducting and Insulating Materials*, Ed. by Z.G. Wang, Y.H. Chen and X.L. Ye (IEEE, New York, 2005) p. 29.
20. Z-Q. Fang, D.C. Look, D.H. Kim, and I. Adesida, "Traps in AlGaIn/GaN/SiC heterostructures studied by deep level transient spectroscopy", *Appl. Phys. Lett.* **87**, 182115, (2005).
21. A. Wyszomolek, R. Stepniowski, M. Potemski, B. Chwalisz, K. Pakula, J.M. Baranowski, D.C. Look, S. S. Park, and K.Y. Lee, "Magnetopolaron effect on silicon and oxygen donor in GaN", 17th International Conference on High Magnetic Fields in Semiconductor Physics, July 30 – Aug 4, 2006.
22. Y. Zhong, K.S. Wong, W. Zhang, and D.C. Look, "Radiative recombination and ultra-long exciton photoluminescence lifetime in GaN freestanding film via two-photon excitation", *Appl. Phys. Lett.* **89**, 022108 (2006).

23. F. Tuomisto, S. Hautakangas, I. Makkonen, V. Ranki, M. J. Puska, K. Saarinen, M. Bockowski, T. Suski, T. Paskova, B. Monemar, X. Xu, and D. C. Look, "Dissociation of $V_{Ga}-O_N$ complexes in HVPE GaN by high pressure and high temperature annealing", *phys. stat. sol. (c)*, accepted.
24. K.P. Korona, A. Wysmolek, J. Kuhl, M. Kaminska, J.M. Baranowski, D.C. Look, and S.S. Park, "Coupling of phonons with excitons bound to different donors and acceptors in hexagonal GaN", *phys. stat. sol. (c)*, accepted.
25. S. Hautakangas, V. Ranki, I. Makkonen, M.J. Puska, K. Saarinen, L. Liskay, D. Seghier, H.P. Gislason, J. Freitas, R.L. Henry, X. Xu, and D.C. Look, "Gallium and nitrogen vacancies in GaN: impurity decoration effects", *Physica B*, accepted.